Model-Based SEI Layer Growth and Capacity Fade Analysis for EV and PHEV Batteries and Drive Cycles

Matthew T. Lawder,[a,*] Paul W. C. Northrop,[b,*] and Venkat R. Subramanian[c,,z]**

[a] *Washington University, St. Louis, Missouri 63130, USA*
[b] *CFD Research Corporation, Huntsville, Alabama 35806, USA*
[c] *Department of Chemical Engineering, University of Washington, Seattle, Washington 98195, USA*

Capacity fade experienced by electric vehicle (EV) and plug-in hybrid electric vehicle (PHEV) batteries will affect the economic and technological value of the battery pack during EV life as well as the value of the battery at the end of life. The growth of the solid-electrolyte interface (SEI) layer is a major cause of capacity fade. We studied the fade caused by SEI layer growth for eight different driving cycles (which include regenerative braking), and six charging protocols. In addition, we looked at the growth caused by varying the depth of discharge during cycling. Constant current and constant current-constant voltage charging patterns at differing rates were studied. Results showed that for half of the driving cycles regenerative braking increased the life-time energy utilization of the battery in addition to increasing the capacity during a single cycle. For the other half of the driving cycles it is shown that while regenerative braking may be beneficial during a single cycle, over the life of the battery it can decrease the total usable energy. These cases were studied using a reformulated porous electrode pseudo two dimensional model that included SEI layer growth as a side reaction.

© The Author(s) 2014. Published by ECS. This is an open access article distributed under the terms of the Creative Commons Attribution Non-Commercial No Derivatives 4.0 License (CC BY-NC-ND, http://creativecommons.org/licenses/by-nc-nd/4.0/), which permits non-commercial reuse, distribution, and reproduction in any medium, provided the original work is not changed in any way and is properly cited. For permission for commercial reuse, please email: oa@electrochem.org. [DOI: 10.1149/2.1161412jes] All rights reserved.

Manuscript submitted March 3, 2014; revised manuscript received July 14, 2014. Published October 3, 2014.

While working electric vehicles (EV) have been in existence for over a century (a lead-acid battery powered car achieved speeds of 30m/s in 1899), the price of EVs has not become competitive with their internal combustion engine (ICE) counterparts.[1] EV sales are currently aided by subsidies ranging from $3,000 in China to $7,500 in the US and Western Europe to $10,000 in Japan.[2] One of the causes of the high prices of EVs is the expensive nature of the vehicle's battery pack, which is not required by ICE vehicles running entirely on gas (hybrids operate on a combination of both systems with plug-in hybrid electric vehicles (PHEV) being able to operate in an all-electric mode). Most currently available and planned EVs (and PHEVs) use a lithium-ion (Li-ion) battery chemistry. Li-ion EV battery pack costs are estimated at between $600-$1,200 per kWh of energy capacity.[2,3] This price can cause battery packs to cost in excess of $10,000 per vehicle and account for 30-50% of total vehicle cost.[4] Decreasing the price of the battery pack will be extremely important in making EVs price competitive in the automobile market.

As EV and PHEVs age, their battery packs will have to be replaced due to capacity and power fade. Power fade is defined as the loss of cell power caused by increased cell impedance from aging. Capacity fade is defined as the loss of energy storage capacity due to degradation caused by cycling.[5] Based on present requirements, EV batteries that have lost 20% of their initial factory capacity are no longer useful for automotive use and should be replaced.[6] Typically, an EV battery will last between 5 to 10 years within its automotive application depending on driving and charging patterns. Nissan estimates that the battery installed in the 2011 Nissan Leaf will contain approximately 80% of its original capacity after five years.[7] PHEV batteries will experience capacity fade on a similar time scale. At the end of the eight year warranty coverage for the Chevrolet Volt's battery, Chevrolet states that the battery may have degraded anywhere between 10% and 30% depending on driving patterns.[8] These wide variations are a by-product of consumer driving and charging patterns. The charging and discharging patterns for EV and PHEVs will greatly affect the amount of capacity fade that occurs during cycling and will determine when the battery needs to be retired from automotive use. While many studies have shown capacity fade associated with SEI layer growth for galvanostatic charge and discharge conditions, few studies have looked at the SEI layer growth caused from dynamic discharge condition seen in EV and PHEVs.[9–11]

Li-Ion Battery Degradation

When attempting to predict the useful life of a battery within an application, the mechanisms that cause a battery to degrade must be understood. Natural degradation of the battery will occur over time regardless of the charge/discharge cycle of the battery. The life-time associated with natural degradation is referred to as "calendar life". Degradation will also occur due to the cyclic charging and discharging of the battery. The life-time associated with the charge/discharge cycle is called "cycle life". Calendar life is an important consideration for applications that have very few cycles spread out over long duration, such as standby power sources, while cycle life is more important for applications going through repeated charge/discharge cycles, such as a cell phone battery.[12] Because EV and PHEV batteries will go through charge/discharge cycles on a daily basis and continue to be used for many years, both cycle and calendar degradation are important in determining the life of the battery throughout automotive use with cycle degradation being the primary reason for failure. This paper is focused only on cycle degradation.

Capacity loss within a Li-ion battery can be caused by many different mechanisms and the relative importance of these various mechanisms is not well understood. Certain factors are known that increase capacity fade such as extreme temperatures, and high charging rates.[13,14] Many different internal mechanisms contribute to capacity fade including mechanical stress effects, which can lead to volume changes, as well as side reactions, which can increase cell resistance and remove active material from the cycling process.[15–18] Side reactions can include many different types of reactions leading to effects such as electrode pore clogging, lithium metal plating or passive layer growth at the electrode-electrolyte interface.[19] These fade mechanisms generally occur during cycling processes, and additional degradation can occur due to calendar fade when the battery is not being cycled. While EVs will experience daily cycling, for a significant portion of the day the vehicle will be sitting idle (not driving or charging).

Empirical approaches for modeling capacity fade have used experimental data and correlated parameter degradation estimation to allow for certain physical parameters that change with each cycle to account for reduced capacity.[18] Semi-empirical approaches have represented

*Electrochemical Society Student Member.
**Electrochemical Society Active Member.
zE-mail: vsubram@uw.edu

Downloaded on 2014-11-13 to IP 128.95.145.3 address. Redistribution subject to ECS terms of use (see ecsdl.org/site/terms_use) unless CC License in place (see abstract).

fade mechanisms such as rate capability loss with equations that are specific to a single battery chemistry and type of cell and use an equation to account for the mechanism causing fade.[11] These approaches work well for a limited number of cases, but lack the robustness to be applied generally.

Theoretical approaches study the physics behind the side reactions within the battery, which are the drivers behind capacity fade. The side reactions occurring at the electrodes have been shown to increase the resistance of the cell, which has been measured experimentally through electrochemical impedance spectroscopy and cyclic voltammetry of highly cycled cells.[20,21] The effects of the increased cell resistance and loss of active lithium can be partly explained by studying the solid-electrolyte interface (SEI) growth. During cycling, a layer of growth forms between the anode and electrolyte. Initially, this layer acts as a protective barrier between the anode and electrolyte, allowing the lithium ions to transfer through the SEI layer to the graphitic anode and intercalate while keeping the electrolyte separated physically from the anode, reducing side reactions along the anode surface and maintaining stability between the anode and electrolyte.[22–24] However after the initial protective layer is formed, the continued growth that occurs during cycling will increase the resistive layer and remove active lithium from the cycling system, thereby lowering the energy and power capacity of the battery. Representations of the reactions causing SEI layer growth have been used to model effects on SOH and remaining capacity.[25] Although many mechanisms contribute to capacity fade, the SEI layer growth has been able to accurately account for overall capacity fade for some chemistries using graphite anodes.[23,24] While this growth can be directly modeled (such as using a kinetic Monte-Carlo simulation), such models have high computational cost requiring large amounts of time for even a small portion of electrode surface.[26]

Modeling SEI layer growth.— The growth of the SEI layer has also been simulated by coupling SEI forming side reactions with the porous electrode pseudo two dimensional model (P2D). Several different expressions have been used to simulate the SEI layer growth and literature has not formed a clear consensus on the most accurate expression. Most of the expressions derive from variations on Butler-Volmer kinetics, with different preexponential dependences on the lithium and solvent concentrations.[11,27,28] A diffusion limited reaction was studied by Pinson and Bazant:[28]

$$j_{SEI} = -k_{SEI} c_{sol}^{0.5} c_{Li^+}^{0.5} \exp\left(\frac{\alpha}{FRT}\left(\Phi_1 - \Phi_2 - U_{SEI} - \frac{\delta}{\kappa_{SEI}}(j_n + j_{SEI})\right)\right) \quad [1]$$

Where the equilibrium potential, U_{SEI}, is not well known with values of 0.4 V and 0.8 V being reported in literature.[29,30] A kinetically limited model was considered by Ramadass, et al. shown as:[11]

$$j_{SEI} = -k_{SEI} \exp\left(\frac{\alpha}{FRT}\left(\Phi_1 - \Phi_2 - U_{SEI} - \frac{\delta}{\kappa_{SEI}}(j_n + j_{SEI})\right)\right) \quad [2]$$

Safari and Delacourt removed the equilibrium potential from the reaction by incorporating its value into the rate constant and assumed the reduction of the solvent to be the rate limiting step in the mechanism shown as:[27]

$$j_{SEI} = -k_{SEI} c_{sol} \exp\left(\frac{\alpha}{FRT}\left(\Phi_1 - \Phi_2 - \frac{\delta}{\kappa_{SEI}}(j_n + j_{SEI})\right)\right) \quad [3]$$

For modeling capacity fade in this paper, we include the effects of the passive layer growth of the SEI layer. By including an additional equation with the P2D battery model for the side reactions that cause the passivation of the SEI layer, we can model the capacity throughout cell life. While many mechanisms are attributed to causing capacity fade, SEI layer growth can be coupled with existing battery models and scaled to accurately simulate capacity fade occurring throughout the cell. The growth of the SEI layer contributes to capacity fade by removing active lithium from the system irreversibly and by increasing the resistance between the solid and liquid phases, creating a layer of lithium carbonate at the SEI.[31] Specifically, the removal of cyclable lithium directly reduces the available capacity, while the increased resistance reduces the power deliverable by the cell. The rate of the side reactions and the growth of the SEI layer are dependent on the local overpotentials and internal concentrations which are directly dependent on the conditions to which the battery is subjected, such as the end of charge cell voltage and charging rate. Side reactions creating the passive SEI layer can form in two steps, at contact of the Li-ion to the electrode and during the intercalation of the Li-ion into the electrode.[32] Additional side reactions that may cause capacity fade, but do not directly contribute to SEI growth, can also occur at these stages.

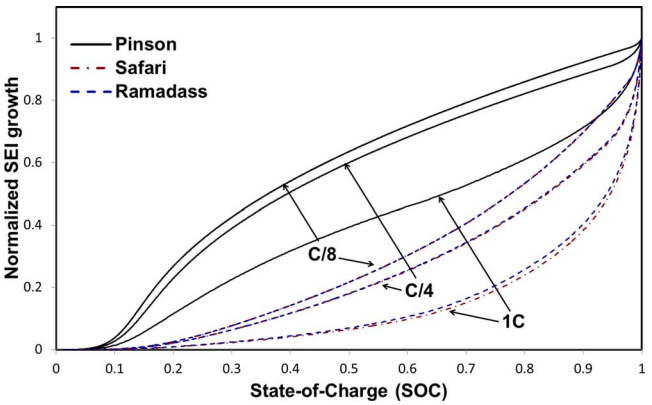

Figure 1. SEI growth shown for charging at 1C, C/4, and C/8 rates for three SEI growth mechanisms. SEI growth is scaled and normalized for the total growth over one charging cycle to be equal across cases.

The SEI layer growth from the three different growth expressions (Eqs. 1–3) can be seen for three charging rates (under constant-current-constant voltage (CC-CV) charging) in Figure 1. Figure 2 shows the SEI growth that occurs during EV use under the dynamic stress test (DST) driving cycle (regenerative charging accounts for almost all of the SEI growth in this case) for all three growth expressions. The kinetically limited expressions from equations 2 and 3 are qualitatively similar, with both showing much greater SEI growth during the later stages of charging, especially the CV portion of charging. As charging rates decrease the differences between the different types of

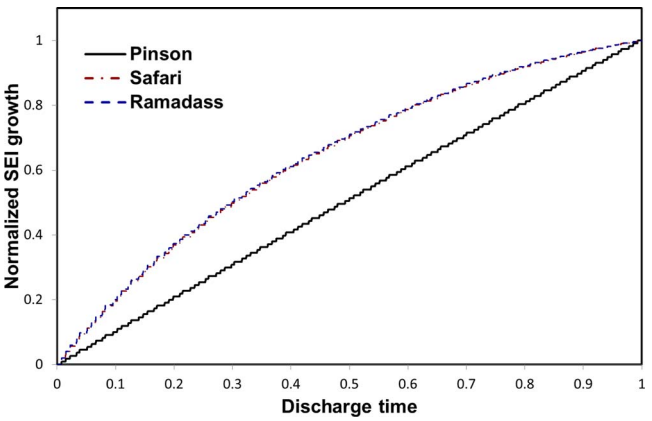

Figure 2. SEI layer growth during the DST driving cycle for each SEI growth mechanism over a complete discharge. Time has been scaled over the entire discharging cycle (Note: Regenerative charging will occur during the driving cycle). SEI growth is scaled and normalized for the total growth over one discharge cycle to be equal across cases.

Downloaded on 2014-11-13 to IP 128.95.145.3 address. Redistribution subject to ECS terms of use (see ecsdl.org/site/terms_use) unless CC License in place (see abstract).

Table I. Percentage of SEI growth from DST driving.

Charging Rate	Percentage of SEI growth from DST driving cycle		
	Pinson and Bazant	*Safari and Delacourt*	*Ramadass, et al.*
1C	6.32%	8.48%	7.54%
C/4	3.07%	6.09%	5.67%
C/8	1.62%	3.60%	3.31%

SEI growth will shrink. Additionally as the charging rate decreases, the ratio of SEI growth occurring during driving to the growth during charging decreases as seen in Table I. Table I shows the percentage of SEI layer growth that occurs during the DST driving cycle when compared to SEI growth from CC-CV charging.

While consumers typically desire fast charging for EV applications, the majority of vehicle charging occurs at levels of 2C and below with Level 2 and home installation charging typically ranging between C/3-and C/16. The charging and discharging occurring during an EV drive cycle can occur in both diffusion limited and kinetically limited regimes because the charging rates will vary depending on the charging site and the discharging and regenerative charging will vary based on driving preferences. However, testing the differences between the SEI growth expressions is beyond the scope of this paper and therefore all simulations beyond this section will utilize the Ramadass, et al. rate expression (Eq. 2). When studying capacity fade over the life of the battery, the amount of growth each cycle is more important than the shape of the growth over a single cycle.

High rates of cycling have been shown to lead to increased capacity fade. However, for the SEI growth expressions shown above, the amount of SEI growth actually increases with a decrease in the charging rate, mainly due to the increased charging time which allows more time for the side reaction to occur.[14] Other mechanisms can have greater effects on capacity fade during high rate charging beyond SEI growth, such as mechanical stress fractures or overcharging.[17] Stress induced fractures can create fresh electrode surface sites which experience greater SEI growth than portions of the electrode that already have some SEI layer covering them.[33,34] At lower rates of charging the contribution of SEI growth toward overall capacity fade is greater and while other fade mechanisms are present, SEI layer growth has been shown to be one of the greatest factors of capacity fade.[19] During driving the C-rate applied to the battery is less than 1 C for 80% of the driving cycle.[35] SEI growth remains an important fade mechanism in the large format cells that are used in electric vehicles.[36,37]

Battery Model (P2D)

We coupled the SEI growth expression with a porous electrode pseudo two dimensional (P2D) model and applied it to EV charging and driving cycles. The P2D model is formulated based on porous electrode and concentrated solution theory along with Ohm's law and battery kinetics, considering the three regions of the battery: the cathode, separator, and anode.[38] Within each region, the P2D model solves for the solid and solution phase concentrations and potentials across the system. The electrodes consist of a solution phase and a solid phase made up of identical spherical particles where diffusion occurs radially. The solution phase is present in all three regions with the concentration and potential varying across the thickness of the cell.[31,39] Fick's second law governs the diffusion of the lithium through the solid spherical particles in both electrodes:

$$\frac{\partial c_i^s}{\partial t} = D_{s,i}\left(\frac{\partial^2 c_i^s}{\partial r^2} + \frac{2}{r}\frac{\partial c_i^s}{\partial r}\right) \qquad i = n, p$$

where c_s is the solid phase lithium concentration, D_s is the diffusion coefficient for the electrode, and i represents either the positive (cathode) or negative (anode) electrode. The intercalation/deintercaltion reaction at the electrode interfaces requires an electronic conduction equation:

$$\sigma_{\text{eff},i}\frac{\partial^2 \Phi_1}{\partial x^2} = a_i F j_i \quad i = n, p$$

where σ_{eff} is the effective conductivity of the electrode, Φ_1 is the solid phase potential, a is the specific surface area of the electrode, F is Faraday's constant, and j is the flux at the electrode-electrolyte interface. The electrode is comprised of single-sized spherical particles. The flux term, j, representative of the reaction at the particle surface, is governed by Butler-Volmerkinetics described as:[40]

$$j_i = 2k_i\left(c^s_{\max,i} - c_i^s\right)^{0.5} c_i^{s0.5} c^{0.5} \sinh\left[\frac{0.5F}{RT}\left(\Phi_1 - \Phi_2 - U_i\right)\right] \quad i = n, p$$

where k is the rate constant for intercalation/deintercalation, c^s_{max} is the maximum solid phase concentration of the electrode, c is the liquid phase Li-ion concentration, R is the gas constant, T is the temperature, Φ_2 is the liquid phase potential, and U is the open circuit potential. Balancing the flow of ions through the electrolyte is a material balance:

$$\varepsilon_i\frac{\partial c}{\partial t} = D_{\text{eff},i}\frac{\partial^2 c}{\partial x^2} + a_i\left(1 - t_+\right) j_i \quad i = n, p$$

where ε is the porosity, D_{eff} is the effective diffusion coefficient of the electrolyte, and t_+ is the transfer number. And a charge balance accounts for the contributions to the total current throughout the cell:[41]

$$-\sigma_{\text{eff},i}\frac{\partial \Phi_1}{\partial x} - \kappa_{\text{eff},i}\frac{\partial \Phi_2}{\partial x} + \frac{2\kappa_{\text{eff},i}RT}{F}\left(1 - t_+\right)\frac{\partial c}{\partial x} = I \quad i = n, p$$

where I is the applied current. These governing equations as well as boundary conditions for the model are shown in Table II.[42]

The physical basis of the P2D model gives it good predictive capabilities over a fairly wide range of conditions,[38] and allows for modifications to include additional physical phenomena, including those which contribute to capacity fade.[28,31,40] However, the detail of the model also increases the computational cost, which makes simulation of a battery throughout its life expensive. In order to solve the model for the entire battery life-time in a reasonable time, simulations for this paper are performed based on a mathematical reformulation of the P2D model developed by Northrop, et al.[43] The reformulated model uses a coordinate transformation and orthogonal collocation to discretize the dependent variables as a series of trial functions, rather than a finite difference approach. In order to develop the required number of equations to determine the coefficients, the governing equations are satisfied at specified node points. These collocation points are chosen as zeroes of orthogonal polynomials to minimize the overall error. In this way, many fewer node points are required to accurately simulate battery performance than if a finite difference scheme were used. The P2D model is important because the local variation of current density means that a 1C rate might create local rates of 3C or higher at the electrode/separator interface.

The P2D model offers a physics-based model that can be easily applied to various chemistries and battery types. While other models have studied fade characteristics for driving cycles, they have utilized equivalent circuit or empirical based models for both the battery and fade dynamics.[44] These models can be effective, but are only valid for a limited number of cases without being empirically refit. Using the P2D model along with a physics-based SEI growth expression creates a more robust simulation tool.

While most of the studies conducted for this paper deal with only one or a few charge-discharge cycles, the use of the reformulated model when studying capacity fade in EVs is critical for cycle life analysis. EV batteries will undergo over a thousand cycles during their use in automotive applications and simulating thousands of charge-discharge cycles, which include stiff driving patterns becomes difficult computationally. Using the reformulated model can greatly reduce the long computational time required for these simulations. Future studies that focus on studying SEI growth and capacity fade over hundreds of cycles will require the computational efficiency of reformulated models.

Downloaded on 2014-11-13 to IP 128.95.145.3 address. Redistribution subject to ECS terms of use (see ecsdl.org/site/terms_use) unless CC License in place (see abstract).

Table II. Equations for the porous electrode pseudo two dimensional model.[43]

Governing Equations

Positive Electrode

$$\varepsilon_p \frac{\partial c}{\partial t} = \frac{\partial}{\partial x}\left[D_{eff,p}\frac{\partial c}{\partial x}\right] + a_p(1-t_+)j_p$$
$$-\sigma_{eff,p}\frac{\partial \Phi_1}{\partial x} - \kappa_{eff,p}\frac{\partial \Phi_2}{\partial x} + \frac{2\kappa_{eff,p}RT}{F}(1-t_+)\frac{\partial \ln(c)}{\partial x} = I$$
$$\frac{\partial}{\partial x}\left[\sigma_{eff,p}\frac{\partial \Phi_1}{\partial x}\right] = a_p F j_p$$
$$\frac{\partial c_p^s}{\partial t} = \frac{1}{r^2}\frac{\partial}{\partial r}\left[r^2 D_p^s \frac{\partial c_p^s}{\partial r}\right]$$

Separator

$$\varepsilon_s \frac{\partial c}{\partial t} = \frac{\partial}{\partial x}\left[D_s \frac{\partial c}{\partial x}\right]$$
$$-\kappa_{eff,s}\frac{\partial \Phi_2}{\partial x} + \frac{2\kappa_{eff,s}RT}{F}(1-t_+)\frac{\partial \ln(c)}{\partial x} = I$$

Negative Electrode

$$\varepsilon_n \frac{\partial c}{\partial t} = \frac{\partial}{\partial x}\left[D_{eff,n}\frac{\partial c}{\partial x}\right] + a_n(1-t_+)j_n$$
$$-\sigma_{eff,n}\frac{\partial \Phi_1}{\partial x} - \kappa_{eff,n}\frac{\partial \Phi_2}{\partial x} + \frac{2\kappa_{eff,n}RT}{F}(1-t_+)\frac{\partial \ln(c)}{\partial x} = I$$
$$\frac{\partial}{\partial x}\left[\sigma_{eff,n}\frac{\partial \Phi_1}{\partial x}\right] = a_n F j_n$$
$$\frac{\partial c_n^s}{\partial t} = \frac{1}{r^2}\frac{\partial}{\partial r}\left[r^2 D_n^s \frac{\partial c_n^s}{\partial r}\right]$$

Boundary Conditions

$$\left.\frac{\partial c}{\partial x}\right|_{x=0} = 0 \qquad \left.\frac{\partial \Phi_1}{\partial x}\right|_{x=l_p^-} = 0$$
$$\left.\frac{\partial \Phi_2}{\partial x}\right|_{x=0} = 0 \qquad \left.\frac{\partial c_p^s}{\partial r}\right|_{r=0} = 0$$
$$\left.\frac{\partial c_p^s}{\partial r}\right|_{r=R_p} = -j_p D_p^s \qquad \left.\frac{\partial \Phi_1}{\partial x}\right|_{x=0} = -\frac{I}{\sigma_{eff,p}}$$
$$-\kappa_{eff,p}\left.\frac{\partial \Phi_2}{\partial x}\right|_{x=l_p^-} = -\kappa_{eff,s}\left.\frac{\partial \Phi_2}{\partial x}\right|_{x=l_p^+}$$
$$-D_{eff,p}\left.\frac{\partial c}{\partial x}\right|_{x=l_p^-} = -D_{eff,s}\left.\frac{\partial c}{\partial x}\right|_{x=l_p^+}$$

$$c|_{x=l_p^-} = c|_{x=l_p^+} \qquad c|_{x=l_p+l_s^-} = c|_{x=l_p+l_s^+}$$
$$\Phi_2|_{x=l_p^-} = \Phi_2|_{x=l_p^+} \qquad \Phi_2|_{x=l_p+l_s^-} = \Phi_2|_{x=l_p+l_s^+}$$

$$\left.\frac{\partial c}{\partial x}\right|_{x=l_p+l_s+l_n} = 0 \qquad \left.\frac{\partial \Phi_1}{\partial x}\right|_{x=l_p+l_s^-} = 0$$
$$\left.\frac{\partial \Phi_2}{\partial x}\right|_{x=l_p+l_s+l_n} = 0 \qquad \left.\frac{\partial c_n^s}{\partial r}\right|_{r=0} = 0$$
$$\left.\frac{\partial c_n^s}{\partial r}\right|_{r=R_p} = -j_n D_n^s \qquad \left.\frac{\partial \Phi_1}{\partial x}\right|_{x=l_p+l_s+l_n} = -\frac{I}{\sigma_{eff,n}}$$
$$-\kappa_{eff,s}\left.\frac{\partial \Phi_2}{\partial x}\right|_{x=l_p+l_s^-} = -\kappa_{eff,n}\left.\frac{\partial \Phi_2}{\partial x}\right|_{x=l_p+l_s^+}$$
$$-D_{eff,s}\left.\frac{\partial c}{\partial x}\right|_{x=l_p+l_s^-} = -D_{eff,n}\left.\frac{\partial c}{\partial x}\right|_{x=l_p+l_s^+}$$

EV Driving Cycles

To study the effects of driving on EV batteries, we apply different standard drive cycles. These cycles incorporate both discharge and regenerative braking, but will be referred to as the discharge portion of battery cycling (charging will refer to only the CC-CV charging of the battery). Eight driving cycles commonly used by the US and European government were chosen. These cycles approximate different types of driving, from urban stop and go cycles to predominately highway cycles. They include: Urban Dynamometer Driving Schedule (UDDS); Federal Test Procedure (FTP-75); Highway Fuel Economy Driving Schedule (HWFET); Supplemental FTP Driving Schedule (US06); Elementary Urban Cycle (ECE-15); Extra-Urban Driving Cycle (EUDC); New European Driving Cycle (NEDC); and DST.[45] Other than the DST cycle, the remaining seven test cycles prescribes a different set of velocities and accelerations throughout the drive cycle. In order to be useful for our studies we must convert these velocity and acceleration time curves into power curves that can then be applied to the EV battery packs.

To find the power required from the battery we need to study the forces that are applied to the car which include:

$$F_{motor} = F_{drive} + F_{rr} + F_{drag} + F_g$$
$$P_{motor} = F_{motor} v$$

Where F_{motor} is the force required from the motor, F_{drive} is the force required for vehicle acceleration, F_{rr} is the rolling resistance between the tires and the roadway, F_{drag} is the force from the aerodynamic drag, and F_g is the gravitational force created when the car is driving uphill or downhill. We will assume for all drive cycles that the driving surface is flat, therefore $F_g = 0$ for all cases.

The three other forces are represented as:[46]

$$F_{drive} = m\frac{dv}{dt}$$
$$F_{rr} = k_r mgcos(\theta)$$
$$F_{drag} = \frac{1}{2}\rho C_D A_f (v - v_w)^2$$

Where m is the vehicle mass, k_r is the rolling resistance coefficient, ρ is the density of air, C_D is the drag force coefficient, A_f is the 2-D projected vehicle area, v_w is the wind velocity (assumed to be zero), and θ is the roadway gradient (also assumed to be zero). Using these conversions we can take any of the normal velocity drive cycles and convert them to power cycles (The only drive cycle that did not need to be converted was the DST cycle, which was developed for EV testing and provides a direct power curve). The vehicle and roadway parameters used to convert vehicle velocity into power are shown in Table III.[47,48] Driving cycles range from the simple ECE-15 seen in Figure 3 to the more reality based UDDS seen in Figure 4.[49,50]

The duration and distance of each driving cycle varies. The driving cycles were repeated multiple times until the battery was 100% discharged. When applying cycles to the battery model with SEI growth, each was scaled so that the battery capacity would allow for 150 km of driving distance, which is a range typical of many available EVs. Therefore the number of individual driving cycles that a battery went through in one discharge varied based on the cycle. The same scaling factor was applied when conducting tests on different depth-of-discharge (DOD) (DOD was calculated based on SOC and anode lithium concentration).

$$SOC = \frac{C_n^s}{C_{\max,n}^s}$$
$$DOD = SOC_{initial} - SOC_{final}$$

EV Charging Characteristics

While fast charging is desired for most EV and PHEVs, a typical EV will see a wide range of different charging patterns over the course of its life-time. Charging rates for EVs are categorized into three levels: Level 1; Level 2; and Level 3. Level 1 charging operates

Table III. Parameters used for converting velocity profiles into power profiles for use in electric batteries.[47,48]

Vehicle Characteristics	
Mass	1500 kg
Coefficient of Drag	0.34
Frontal Area	1.75 m^2
Regenerative Efficiency	0.6
Tire rolling drag coefficient	0.01

Downloaded on 2014-11-13 to IP 128.95.145.3 address. Redistribution subject to ECS terms of use (see ecsdl.org/site/terms_use) unless CC License in place (see abstract).

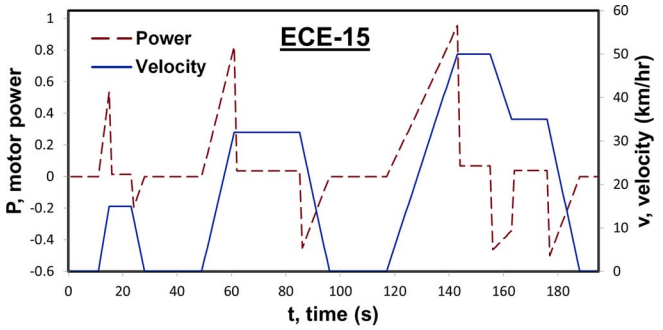

Figure 3. The power and velocity seen under vehicle conditions shown in Table IV for the ECE-15 drive cycle.

through the standard residential outlet plug (120 V AC) and EVs will have the charging equipment built in to the vehicle. This type of charging will only add a few miles of charge per hour. Therefore, it can take over ten hours to fully charge a vehicle depending on the battery size and is typically only used for residential overnight charging. Level 2 charging occurs at mid-range voltages (208 V and 240 V (AC) are common levels) and requires off-board charging equipment. This level of charging is prominent in public charging stations or can be installed in homes. Charging at Level 2 takes between 2-8 hours. Level 3 encompasses charging rates that can fully charge a battery in even less time through use of DC often at 480 V (Note that the AC/DC refers only to the charging source, the battery must be charged through DC). These charging stations require extensive off-board equipment, but offer the ability to regain close to a full charge in a half hour. Note that all charging times are dependent on battery size. The range of rates that typical EV batteries experience is between C/8-2C. Figure 5 shows the differing SEI growth over one cycle of charging followed by the DST driving cycle at these different charging rates. Vehicle charging will lead to the majority of growth over the life of battery.

Results and Discussion

Most charging applications apply a constant current charge followed by a constant voltage charge (CC-CV). While this protocol maximizes the amount of charge stored for a single cycle, the CV portion of charging greatly increases the charging time while adding stored charge at a diminishing rate. The increased charging time will lead to increased SEI growth. CV charging only occurs during the end of the charging cycle and at high levels of SOC. Figure 1 shows that during the CV portion of charging the rate of SEI growth with respect to charge stored increases for all cases. Previous experimental studies have shown that increasing the portion of CV charging can lead to increased capacity fade.[51] In cases where a EV owner is willing to forego the additional charge stored from CV charging (less than 10% in most cases), they will see a benefit over the life of the battery by

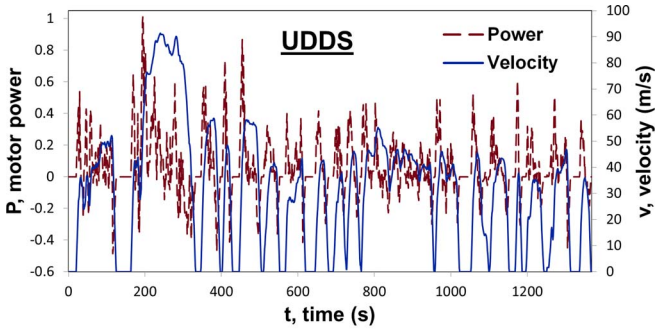

Figure 4. The power and velocity seen under vehicle conditions shown in Table IV for the UDDS drive cycle.

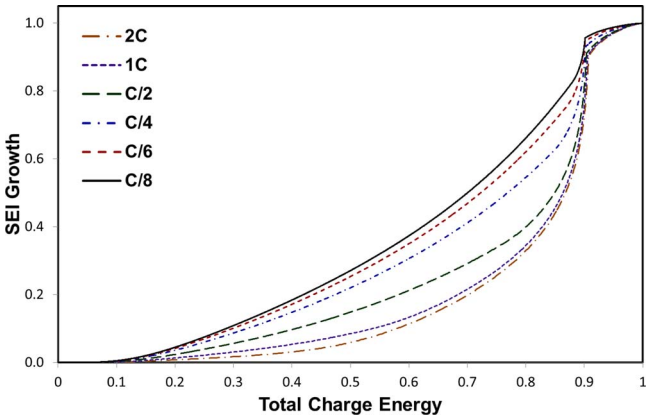

Figure 5. SEI growth over a single charge/discharge cycle, for six different rates of CC-CV charging. The discharge cycle in all cases was the standard DST driving cycle. "Total Charge Energy" is scaled based on the total amount of energy used to charge the battery (including regenerative charging during the discharge cycle). SEI growth is scaled and normalized for the total growth over one charge-discharge cycle to be equal across cases.

reducing the SEI growth. Other degradation effects may negate the benefit of CC only charging.

An overview of several EV and PHEVs available to the public in 2013 is shown in Table IV. This table includes all EVs and PHEVs that sold at least 550 units in the US during 2013. For the two types of vehicles reviewed here (EV and PHEV), the charge/discharge patterns vary. PHEVs can operate in several modes depending on how the driver wishes to use the available capacity. In a charge depleting mode, the PHEV battery will experience deep DOD cycles because the battery will be completely depleted as the vehicle operates in an all electric mode until the battery is out of energy and then switches to the ICE. A more commonly used mode for PHEVs is a charge sustaining mode which will keep the battery capacity at an average capacity during driving through sparingly using the electric motor in combination with the ICE. The vehicle will only operate in all-electric mode for a portion of its battery capacity before switching to a balance between the ICE and battery.

Many PHEV batteries are optimally sized so that a consumer's average driving cycle will use the entire battery capacity while only briefly needing the ICE. The DOD patterns of PHEVs will often experience deeper DOD than EVs because of their smaller battery size (although charge sustaining operation for PHEVs will limit the DOD). An EV's battery is sized to allow for cushion or buffer capacity beyond the consumer's typical driving cycle so that a driver is not stranded on the road. This overhead capacity is rarely used, but does alleviate some of the consumer's range anxiety (fear that the vehicle will not be able to travel to a desired destination and back on a single charge) which is one of the primary customer concerns when purchasing an EV.[52–54]

For PHEVs, battery sizing is based on capturing the optimal amount of vehicle miles. Vehicle manufactures differ on what is viewed as optimal size shown in the great variance of battery capacity present among PHEVs in Table IV. The Department of Transportation determined that the average trip distance for a US vehicle in 2009 was 9.72 miles and the average daily vehicle miles traveled (VMT) per driver was 28.97 miles.[55] Figure 6 shows the percentage of miles covered in all electric mode for several of the PHEVs and Figure 7 shows the amount average miles driven per vehicle.[56,57]

The daily driving cycles will affect the DOD experienced by EVs and PHEVs. Assuming operation in all electric mode for the entire battery capacity (no charge sustaining mode or re-charging), a battery with a 10 mile all-electric range will experience 100% DOD during 96% of an average driver's daily travel cycles, while a battery with a 40 mile all-electric range will experience full discharge in only 69% of daily travel cycles. Variation in DOD cycles creates more

Downloaded on 2014-11-13 to IP 128.95.145.3 address. Redistribution subject to ECS terms of use (see ecsdl.org/site/terms_use) unless CC License in place (see abstract).

Table IV. Characteristics of 2013 production EV batteries.[8,62–69]

Car Type	Make	Model	Energy Capacity (kWh)	Range (miles)	MPGe	Peak Power (kW)	MSRP ($)
EV	Fiat	500 e	24	87	108	83	31800
	Ford	Focus EV	23	76	105	107	39200
	Honda	Fit EV	20	82	118	100	37415[b]
	Mitsubishi	i-MiEV	16	62	112	49	29975
	Nissan	Leaf	24	75	115	80	28800
	Smart	ED	17.6	68	107	55	25000
	Tesla	Model S	60/85	208/265	95/89	270/270	69900/79900
	Toyota	Rav4 EV	41.8	103	76	115	49800
PHEV	Chevy	Volt	16.5	38	98	111	39145
	Ford	Fusion Energi	7.6	21	100	88	35525
	Ford	C-max Energi	7.6	21	100	88	33745
	Toyota	Prius Plug-in	4.4[a]	11	95	60	32000

[a]The Prius-Plug-in energy capacity is an estimated amount.
[b]The Honda Fit EV is only available to lease.

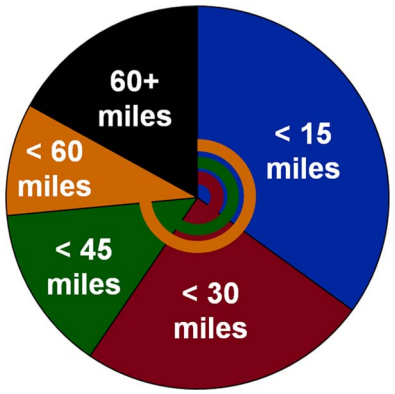

Figure 6. Amount of daily VMT for American vehicles. Blue represents all vehicles driven less than 15 miles per day. Blue and Red represent all vehicles driven less than 30 miles per day, etc.

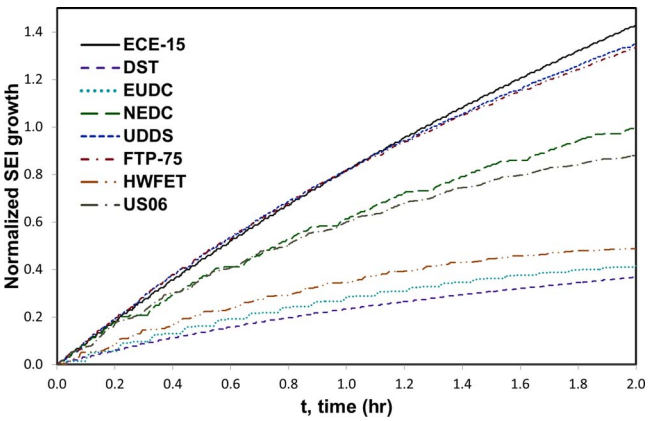

Figure 8. SEI growth for all 8 driving cycles for two hours of driving. The SEI growth was scaled to the amount of growth from the NEDC case over two hours in order to show a relative comparison among the driving cycles.

difficulty for vehicle manufactures who try to implement a BMS to optimally control the battery.[58] While PHEVs will experience deep discharge more frequently, EVs will still utilize a larger absolute amount of battery energy due to the greater size of their battery and the requirement that all VMT are driven by electric power. The nature of an individual's driving cycles and the amount of regenerative braking that occur during a cycle will also affect the vehicle's all electric range and the battery's experienced DOD.

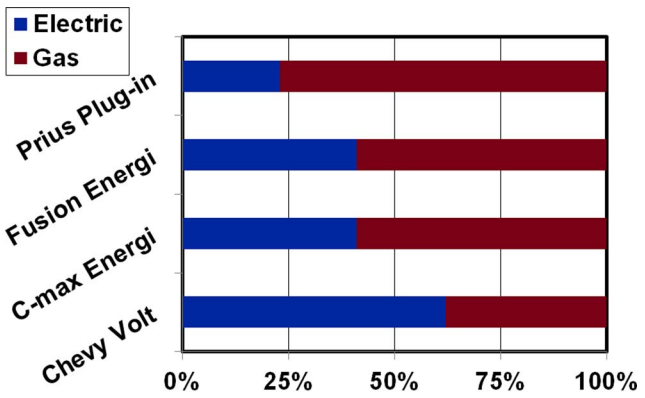

Figure 7. Percentage of total VMT driven using the all-electric mode for different PHEV models (assuming charge depletion).

SEI growth results.— We applied each of the driving cycle power curves to the P2D Li-ion battery model with SEI layer growth to study the effects of different driving patterns and different levels of regenerative braking on the SEI layer growth within the battery. Figures 8 and 9 show the SEI layer growth during the first two hours of driving and the first 30 km of distance covered, respectively. The

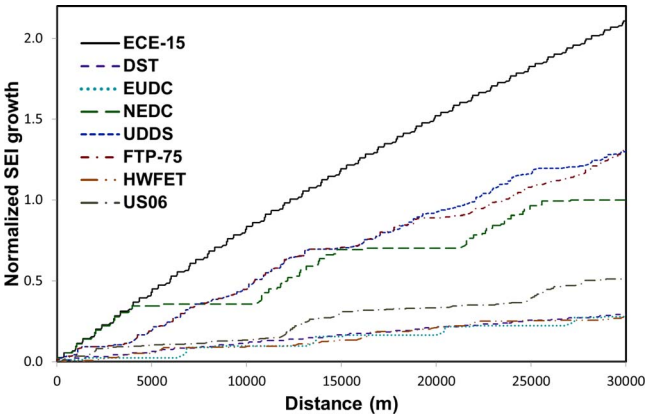

Figure 9. SEI growth for all 8 driving cycles for 30 km of driving. The SEI growth was scaled to the amount of growth from the NEDC case over 30 km in order to show a relative comparison among the driving cycles.

Downloaded on 2014-11-13 to IP 128.95.145.3 address. Redistribution subject to ECS terms of use (see ecsdl.org/site/terms_use) unless CC License in place (see abstract).

Table V. Drive cycle characteristics. *Regen Energy Added* is the percentage of energy gained from regenerative braking during the driving cycle compared to the amount of energy stored during normal charging. *Regen SEI Added* is the percentage of SEI layer growth gained from regenerative braking compared to the growth for a single charge. SEI growth/min and SEI growth/km are scaled to the amount of SEI growth/min and SEI growth/km of the NEDC cycle, respectively.

EV Cycle	DST[a]	NEDC	ECE-15	EUDC	UDDS	FTP-75	HWFET	US06
Average Velocity (km/h)	46.3	33.6	18.4	62.6	31.5	34.2	77.7	77.9
Duration (min)	6.0	19.7	3.3	6.7	22.8	31.2	12.8	9.9
Distance (km)	4.63	11.02	1.00	6.96	11.99	17.79	16.45	12.89
Regen Energy Added	18.1%	18.2%	66.6%	15.9%	49.1%	41.0%	27.1%	50.0%
Regen SEI Added	11.7%	39.0%	82.9%	11.3%	54.2%	51.2%	12.8%	23.1%
R-P Ratio	0.052	0.183	0.423	0.143	0.363	0.357	0.171	0.303
SEI growth/min	0.37	1.00	1.38	0.43	1.38	1.39	0.54	0.97
SEI growth/km	0.29	1.00	2.14	0.29	1.43	1.37	0.32	0.58

[a]DST characteristics for velocity and distance were back calculated from the DST's power curve.

SEI growth in these figures has been normalized relative to the amount of growth experienced under the NEDC driving cycle during the same periods. The absolute values of SEI layer growth are on the order of nanometers as only one cycle was simulated.[59,60]

The results show that the drive cycles that averaged faster speeds and had lower ratios of regenerative braking power to propulsion power (R-P ratio) also had lower amounts of growth during the driving cycle. This trend held for both SEI growth measured over distance traveled and over time. The distribution among rates was much greater for the rate per distance traveled than it was from time. Results for the amount of growth per unit distance and per unit time of each cycle are shown in Table V. For each drive cycle the duration and magnitude of the acceleration and deceleration period were the predominant factors in determining the ratio of regenerative power that could be captured (shown Table V). Stretches of constant velocity did not affect the power, but did increase the distance traveled greatly with less growth of the SEI layer. Cycles such as the HWFET cycle which maintains a high constant velocity without much acceleration, travels longer distances without gaining as much SEI layer growth as other cycles. In general, the cycles that approximate lower speed, urban driving patterns experienced more SEI growth during an entire discharge cycle, but also had the greatest amount of regenerative braking (which is the main cause for SEI growth during driving) and therefore would typically require a smaller battery pack in order to achieve the distances studied. Additionally, when driving between points, utilizing driving patterns similar to the DST or EUDC cycles (which experience the lowest growth rates per km) would be most beneficial for reducing SEI growth.

When focusing on how the regenerative nature of the driving cycle affects the amount of SEI growth, we found the percentage of additional energy output from the battery and the amount of additional SEI layer growth during a single discharge cycle caused from using regenerative braking instead of conventional brakes (see Table V). While the regenerative braking caused some SEI formation for all the drive cycles, the cycles that experienced the greatest amount of additional energy benefit also experienced the greatest rate of SEI growth. For the ECE-15, UDDS, FTP-75, and NEDC cycles, the percentage of additional SEI growth exceeded the additional energy gained. If SEI growth was the only fade mechanism occurring during driving, then the use of regenerative braking during these cycles would be prohibitive over the entire life of the battery because even though additional energy is being gained during a single cycle, the fade that occurs will result in a net total energy loss over the life of the battery due to the decrease in cycle life. For the DST, EUDC, HWFET, US06 cycles the additional percentage of energy gained is greater than the additional SEI layer growth meaning that the use of regenerative braking in these cycles is beneficial over both a single cycle and the entire life of the battery. Experimental results for the DST cycle show that the addition of regenerative breaking does offer a life-time benefit.

Figure 10 shows Li-ion 18650 cells ($LiFePO_4$) charged under 1C CC-CV protocol and discharged (100% DOD) under the DST driving cycles with conventional breaking (no recharge during the discharge cycle) and regenerative braking. Tests were conducted over 1000 cycles for both cases. After 1000 cycles both cases had lost similar amounts of capacity with the regenerative case losing 4.45% and the non-regenerative case losing 4.46%. But due to charging during braking, the regenerative case discharged a greater amount of energy per charge/discharge cycle than the conventional braking case. Therefore over 1000 cycles the regenerative braking case had discharged 15.7% more energy and had equivalent capacity remaining. Under the DST cycle, regenerative braking is beneficial over the lifetime of the battery.

Many real-world driving cycles do not deplete the battery to 100% DOD before recharging. We looked at the SEI growth of cycling at different DOD levels for each of the driving cycles. The results for SEI growth at 4 different DOD levels is shown in Figure 11 for the HWFET cycle and Figure 12 for the UDDS cycle. Figures 11–13 only show SEI growth during discharging (no charging growth). The SEI growth for these figures is measured in comparison to the amount of discharged energy since more energy will be discharged during deeper DOD (and more SEI growth would therefore be expected). This method allows for comparison between cases even though different amounts of energy were stored during a single cycle. The discharge energy and SEI growth for the three figures is scaled to the amount caused by two cycles at 100% DOD. Table VI summarizes the relative SEI layer growth for all the driving cycles based on varying DOD where the amount of usable energy from the batteries is normalized to the

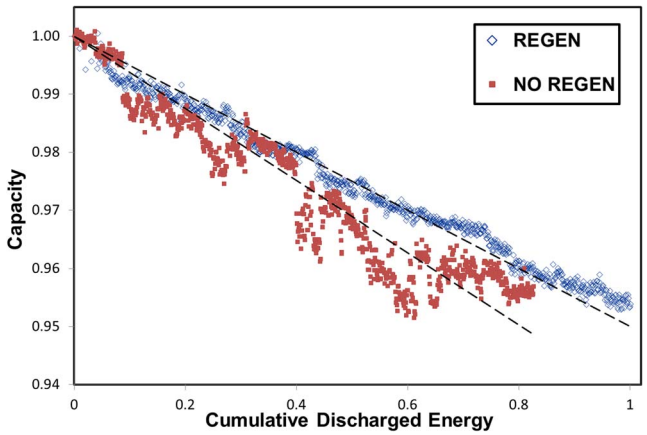

Figure 10. Experimental data comparing the use of regenerative braking in the DST cycle. Both cases were charged using a 1C CC-CV charging pattern and discharged using the DST driving cycle. However in the "No Regen" case the regenerative braking portions of the DST cycle were removed and replaced with rest periods (i.e. conventional braking system). Both cases were run for 1000 cycles. Cumulative Discharged Energy is normalized for the output from 1000 cycles for the Regen case.

Downloaded on 2014-11-13 to IP 128.95.145.3 address. Redistribution subject to ECS terms of use (see ecsdl.org/site/terms_use) unless CC License in place (see abstract).

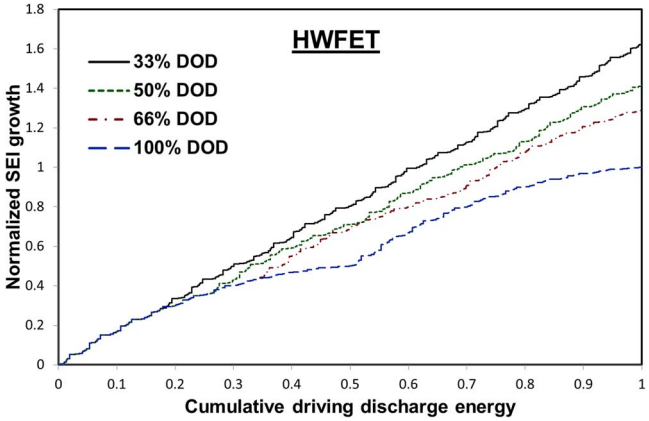

Figure 11. SEI growth over multiple driving cycles using the HWFET driving cycle for differing DOD. For all cases discharge will begin at 100% SOC.

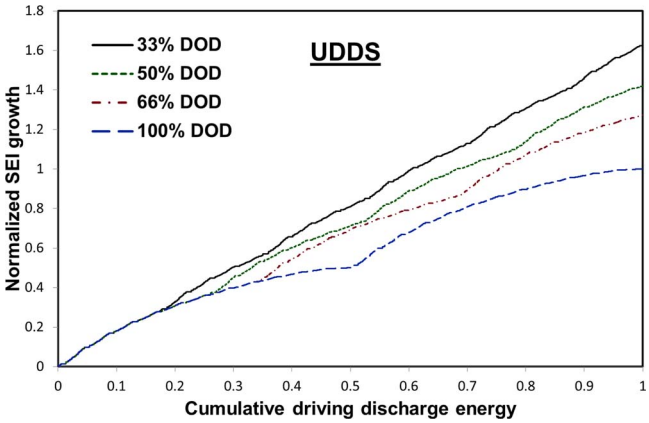

Figure 12. SEI growth over multiple driving cycles using the UDDS driving cycle for differing DOD. For all cases discharge will begin at 100% SOC.

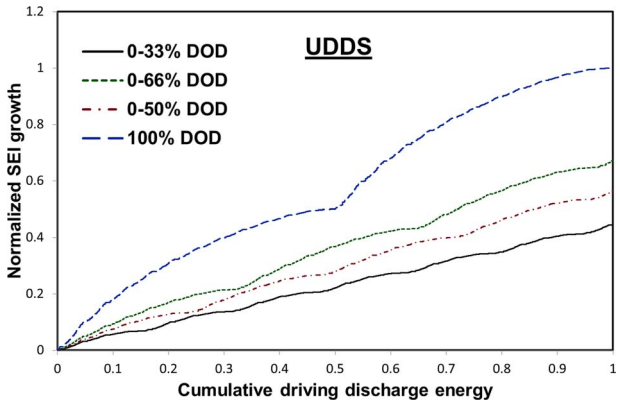

Figure 13. SEI growth over multiple driving cycles using the UDDS driving cycle for differing DOD. For all cases discharge will end at 0% SOC.

amount of energy utilized during two 100% DOD discharges. The SEI growth is greater for cycling at lower DOD for all of the driving cycles. Part of this higher growth rate is due to the higher potential of the battery during cycling for small DOD cycles because lower potentials correlate to the lower states of charge. Figures 11 and 12 and Table VI have measured DOD starting from 100% SOC, however we can also start the driving cycle at a lower state of charge. For example, instead of beginning a 33% DOD at 100% SOC and driving until 67% SOC, the driving cycle can begin at 33% SOC and end at 0% SOC.

Table VI. Ratio of SEI layer growth over the equivalent energy output for different DOD to 100% DOD for all eight driving cycles beginning at 100% SOC for all cases.

	SEI growth normalized to 100% DOD case		
Driving Cycle	*66% DOD*	*50% DOD*	*33% DOD*
DST	1.30	1.45	1.68
NEDC	1.31	1.47	1.69
ECE-15 (UDC)	1.30	1.46	1.68
EUDC	1.29	1.47	1.64
UDDS	1.27	1.42	1.62
FTP-75	1.23	1.36	1.54
HWFET	1.29	1.42	1.64
US06	1.22	1.36	1.52

Changing the range of SOC experienced during driving will change the potential of the battery during the cycle. Results for the same 4 DOD for the UDDS cycle are again shown in Figure 13, however now the SOC range will always go to 0% SOC (eg. 0-33% SOC, 0-50% SOC, 0-67% SOC). Because of the lower potential during the driving cycles the SEI growth is actually lowest for the 100% DOD case on a growth per km driven basis. Since the EV cycles apply a desired power to the battery, the current applied by the cycles will be higher during the operation at low SOCs. However, Figure 13 shows that the potential is more important for the SEI growth than the applied current. Experimental studies have shown increased side reactions at the SEI layer for high potentials.[61]

Although operating the battery at lower SOC will reduce the SEI growth, it has several other undesirable affects. Along with increases in the current needed to meet power requirements, low SOC operation does not utilize the full capacity of the battery. In most EV cases, drivers will begin the day with a full charge at 100% SOC and therefore cycling beginning at low SOC levels would not be commonly seen in EV usage.

When studying the complete life-time of the battery, simulations will need to include multiple years of driving cycles and run until the end of automotive life. These simulations must include hundreds to thousands of cycles. While studying the end of life characteristics of batteries is beyond the scope of this paper, Figure 14 shows the ability of the reformulated model to approach these types of problems. Figure 14 shows the SEI layer growth for 500 charge/discharge cycles for the HWFET, NEDC, and UDDS driving cycles. These simulations required 6.54, 4.56, and 7.49 hours respectively to complete 500 cycles. Without using the reformulated model each of these cases would

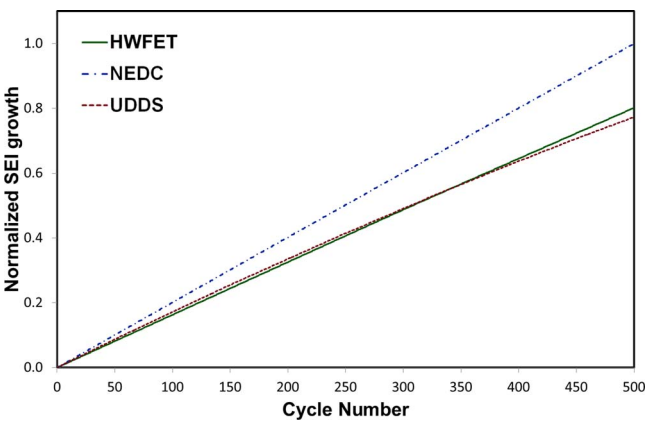

Figure 14. SEI growth over 500 charge/discharge cycles (100% DOD) for the HWFET, NEDC, and UDDS driving cycles. The SEI growth was scaled to the amount of growth from the NEDC case over 500 cycles in order to show a relative comparison among the driving cycles.

Downloaded on 2014-11-13 to IP 128.95.145.3 address. Redistribution subject to ECS terms of use (see ecsdl.org/site/terms_use) unless CC License in place (see abstract).

have required multiple days to weeks for running a single simulation. The use of the reformulated P2D model enhances the efficiency for solving stiff computational problems such as EV driving. Figure 14 also shows that continuing to drive under the NEDC driving cycle will lead to more total SEI layer growth than driving under the HWFET or UDDS over 500 cycles.

Conclusions

Passive SEI layer growth is a major contributor to capacity fade in Li-ion batteries used for EV and PHEV applications. The majority of SEI layer growth will occur during charging. While fast charging creates undesired stress and temperature affects among other degradation problems, it will limit the amount of direct SEI layer growth in comparison to slow rates. Additionally, CC-CV charging will increase the amount of charge stored within a battery for a single cycle, but over the entire cycle life of the battery will decrease the total amount of usable energy from the battery for drive cycle cases.

The driving cycle will add to the SEI layer growth mainly during the regenerative braking portion of the drive cycles. For start and stop traffic, where most driving occurs at low speeds, the negative effect of SEI layer growth on cycle life exceeds the benefit of increased energy available to the driver during a single cycle. If regenerative braking is used in these cases, the total amount of usable energy over the life of the battery will decrease. For driving cycles that have higher, more constant speeds, and briefer (sharper) levels of deceleration, the SEI layer grows at a slower rate than the amount of energy added, which results in benefits over both a single cycle and the life-time of the battery.

During daily cycling most EVs do not experience a 100% DOD of their batteries. Cycling at smaller DOD from 100% SOC will increase the amount of SEI growth per mile driven compared to 100% DOD cycling. However, cycling at small DOD at lower starting SOC (eg. starting at 50% SOC and cycling to 0% SOC for a 50% DOD) will decrease the amount of SEI layer growth when compared to 100% DOD mainly due to the lower battery potential during cycling. While cycling at lower SOC may be beneficial for reducing SEI growth, it is not advisable for actual EV and PHEV use because it causes underutilization of the battery capacity over each cycle.

Acknowledgments

Simulation work was accomplished using MAPLE and MAPLESim. Codes are available upon request.

This paper is based upon work supported in part under the US-India Partnership to Advance Clean Energy-Research (PACE-R) for the Solar Energy Research Institute for India and the United States (SERIIUS), funded jointly by the U.S. Department of Energy (Office of Science, Office of Basic Energy Sciences, and Energy Efficiency and Renewable Energy, Solar Energy Technology Program, under Subcontract DE-AC36-08GO28308 to the National Renewable Energy Laboratory, Golden, Colorado) and the Government of India, through the Department of Science and Technology under Subcontract IUSSTF/JCERDC-SERIIUS/2012 dated 22nd Nov. 2012.

List of Symbols

c	liquid phase lithium ion concentration
c^s	solid phase lithium concentration
j	Pore wall flux (determined from Butler-Volmer kinetics)
t_+	Transference number
a	Particle surface area to volume
D_{eff}	Effective Electrolyte Diffusivity
D^s	Solid Phase Diffusivity
Φ_1	Solid phase potential
Φ_2	Liquid phase potential
σ_{eff}	Solid phase conductivity
κ_{eff}	Liquid phase conductivity
ε	Bruggeman Coefficient
I	Applied Current
R	Gas Constant
T	Temperature
F	Faraday's Constant
c_{sol}	Concentration of solvent at anode surface
c_{Li+}	Concentration of lithium at anode surface
k_{SEI}	rate constant for SEI reaction
α	transfer coefficient
U_{SEI}	SEI equilibrium potential
δ	SEI layer thickness
κ_{SEI}	Conductivity of SEI layer
j_{SEI}	flux associated with SEI layer growth
j_n	flux associated with normal intercalation at the anode
C_D	aerodynamic drag coefficient of vehicle
A_f	Front projected area of vehicle
m	mass of vehicle
g	acceleration of gravity
k_r	coefficient of rolling resistance
v	velocity of vehicle
ρ	density of air
F_{force}	Force on vehicle

References

1. M. Armand and J. M. Tarascon, *Nature*, **451**, 652 (2008).
2. A. Dinger, R. Martin, X. Mosquet, M. Rabl, D. Rizoulis, and M. Russo et al., "Batteries for Electric Cars: Challenges, Opportunities, and the Outlook to 2020," Boston Consulting Group 2010.
3. J. Nuebauer, A. Brooker, and E. Wood, *Journal of Power Sources* **209**, 269 (2012).
4. R. Allen, *Electronic Design* **3/26**, 26 (2010).
5. B. Pattipati, C. Sankavaram, and K. R. Pattipati, *Ieee Transactions on Systems Man and Cybernetics Part C-Applications and Reviews*, **41**, 869 (2011).
6. E. Cready, J. Lippert, J. Pihl, I. Weinstock, P. Symons, and R. G. Jungst, "Technical and economic feasibility of applying used EV batteries in stationary applications," Sandia National Labs 2003.
7. Nissan. 2011 Leaf Owner's Manual. *Nissanusa.com.* nissan-techinfo.com/refgh0v/og/leaf/2011-nissan-leaf.pdf, last accessed: March 2011.
8. Chevrolet. *Chevrolet*. www.chevrolet.com, last accessed: May 2013.
9. P. Ramadass, B. Haran, R. White, and B. N. Popov, *Journal of Power Sources*, **123**, 230 (2003).
10. A. P. Schmidt, M. Bitzer, A. W. Imnre, and L. Guzzella, *Journal of Power Sources*, **195**, 7634 (2010).
11. P. Ramadass, B. Haran, P. M. Gomadam, R. White, and B. N. Popov, *Journal of the Electrochemical Society*, **151**, A196 (2004).
12. M. Broussely, S. Herreyre, P. Biensan, P. Kasztejna, K. Nechev, and R. J. Staniewicz, *Journal of Power Sources*, **97-8**, 13 (2001).
13. I. Bloom, B. W. Cole, J. J. Sohn, S. A. Jones, E. G. Polzin, and V. S. Battaglia et al., *Journal of Power Sources*, **101**, 238 (2001).
14. G. Ning, B. Haran, and B. N. Popov, *Journal of Power Sources*, **117**, 160 (2003).
15. Y. Hamon, T. Brousse, F. Jousse, P. Topart, P. Buvat, and D. M. Schleich, *Journal of Power Sources*, **97-8**, 185 (2001).
16. I. Kim, G. E. Blomgren, and P. N. Kumta, *Electrochemical and Solid State Letters*, **6**, A157 (2003).
17. P. Arora, R. E. White, and M. Doyle, *Journal of the Electrochemical Society* **145-10**, 3647 (1998).
18. V. Ramadesigan, K. J. Chen, N. A. Burns, V. Boovaragavan, R. D. Braatz, and V. R. Subramanian, *Journal of the Electrochemical Society*, **158**, A1048 (2011).
19. M. Broussely, P. Biensan, F. Bonhomme, P. Blanchard, S. Herreyre, and K. Nechev et al., *Journal of Power Sources*, **146**, 90 (2005).
20. J. Vetter, P. Novak, M. R. Wagner, C. Veit, K. C. Moller, and J. O. Besenhard et al., *Journal of Power Sources*, **147**, 269 (2005).
21. D. Zhang, B. S. Haran, A. Durairajan, R. E. White, Y. Podrazhansky, and B. N. Popov, *Journal of Power Sources*, **91**, (2000).
22. V. Etacheri, R. Marom, R. Elazari, G. Salitra, and D. Aurbach, *Energy & Environmental Science*, **4**, 3243 (2011).
23. R. Spotnitz, *Journal of Power Sources*, **113**, 72 (2003).
24. S. Bashash, S. J. Moura, J. C. Forman, and H. K. Fathy, *Journal of Power Sources*, **196**, 541 (2011).
25. A. V. Randall, R. D. Perkins, X. C. Zhang, and G. L. Plett, *Journal of Power Sources*, **209**, 282 (2012).
26. R. N. Methekar, P. W. C. Northrop, K. J. Chen, R. D. Braatz, and V. R. Subramanian, *Journal of the Electrochemical Society*, **158**, A363 (2011).

Downloaded on 2014-11-13 to IP 128.95.145.3 address. Redistribution subject to ECS terms of use (see ecsdl.org/site/terms_use) unless CC License in place (see abstract).

27. M. Safari, M. Morcrette, A. Teyssot, and C. Delacourt, *Journal of the Electrochemical Society*, **156**, A145 (2009).
28. M. B. Pinson and M. Z. Bazant, *Journal of the Electrochemical Society*, **160**, A243 (2013).
29. A. Naji, J. Ghanbaja, B. Humbert, P. Willmann, and D. Billaud, *Journal of Power Sources*, **63**, 33 (1996).
30. G. Sikha, B. N. Popov, and R. E. White, *Journal of the Electrochemical Society*, **151**, A1104 (2004).
31. S. Santhanagopalan, Q. Z. Guo, P. Ramadass, and R. E. White, *Journal of Power Sources*, **156**, 620 (2006).
32. S. S. Zhang, *Journal of Power Sources*, **162**, 1379 (2006).
33. S. Bhattacharya, A. R. Riahi, and A. T. Alpas, *Journal of Power Sources*, **196**, 8719 (2011).
34. J. Christensen, *Journal of the Electrochemical Society*, **157**, A366 (2010).
35. S. B. Peterson, J. Apt, and J. F. Whitacre, "Lithium-ion battery cell degradation resulting from realistic vehicle and vehicle-to-grid utilization," *Journal of Power Sources*, **195**, 2385 (2010).
36. M. Dubarry, B. Y. Liaw, M. S. Chen, S. S. Chyan, K. C. Han, and W. T. Sie et al., *Journal of Power Sources*, **196**, 3420 (2011).
37. Y. C. Zhang, C. Y. Wang, and X. D. Tang, *Journal of Power Sources*, **196**, (2011).
38. M. Doyle, T. F. Fuller, and J. Newman, *Journal of the Electrochemical Society*, **140**, (1993).
39. V. Ramadesigan, P. W. C. Northrop, S. De, S. Santhanagopalan, R. D. Braatz, and V. R. Subramanian, *Journal of the Electrochemical Society*, **159**, S12 (2012).
40. G. G. Botte, V. R. Subramanian, and R. E. White, *Electrochimica Acta*, **45**, 2595 (2000).
41. C. Y. Wang, W. B. Gu, and B. Y. Liaw, *Journal of the Electrochemical Society*, **145**, (1998).
42. V. R. Subramanian, V. Boovaragavan, V. Ramadesigan, and M. Arabandi, *Journal of the Electrochemical Society*, **156**, A260 (2009).
43. P. W. C. Northrop, V. Ramadesigan, S. De, and V. R. Subramanian, *Journal of the Electrochemical Society*, **158**, A1461 (2011).
44. J. Nuebauer and E. Wood, *Journal of Power Sources*, **259**, 262 (2014).
45. Environmental Protection Agency. *Dynamometer Drive Schedules*. http://www.epa.gov/nvfel/testing/dynamometer.htm, last accessed: March 2014.
46. R. V. N. Melnik, N. Song, and P. Sandholdt, "Dynamics of torque-speed profiles for electric vehicles and nonlinear models based on differential-algebraic equations," in *Proceedings of the Fourth International Conference on Dynamical Systms and Differential Equations*, Wilmington, NC, USA, 2002.
47. Committee for the national Tire Efficiency Study, "Tires and Passenger Fuel Economy: Improving Consumers, Improving Performance," National Research Council of the National Academies 2006, 2006.
48. Y. Gao, L. Chu, and M. Ehsani, "Design and control principles of hybrid braking system for EV and FCV," presented at the *Vehicle Power and Propulsion Conference*, Arlington, TX, 2007.
49. Environmental Protection Agency. *Dynamomter Drive Schedules*. http://www.epa.gov/nvfel/testing/dynamometer.htm, last accessed: March 2014.
50. T. J. Barlow, S. LAtham, I. S. McCrae, and P. G. Boulter. (2009). *A reference book of driving cycles for use in the measurement of road vehicle emissions*.
51. G. Sikha, P. Ramadass, B. S. Haran, R. E. White, and B. N. Popov, *Journal of Power Sources*, **122**, 67 (2003).
52. M. K. Hidrue, G. R. Parsons, W. Kempton, and M. P. Gardner, *Resource and Energy Economics*, **33**, 686 (2011).
53. International Energy Agency, Electric Vehicles Initiative, and C. E. Ministerial, "Global EV Outlook: Understanding the Electric Vehicle Landscape to 2020," International Energy Agency April, 2013, 2013.
54. J. Nuebauer and E. Wood, *Journal of Power Sources*, **257**, 12 (2014).
55. A. Santos, N. McGuckin, H. Y. Nakamoto, D. Gray, and S. Liss, "Summary of Travel Trends 2009 National Houshold Travel Survey," 2011.
56. A. Vyas and D. Santini, "Use of National Surveys for Estimating "Full" PHEV Potential for oil use reduction," presented at the PLUG-IN 2008 Conference, San Jose, CA, 2008.
57. NHTS. *National Household Travel Survey*. nhts.ornl.gov, last accessed: March 2014.
58. A. Vyas and D. Santini, *PLUG-IN 2008 Conference, San Jose, CA*, (2008).
59. W. Choi, J. Y. Lee, B. H. Jung, and H. S. Lim, *Journal of Power Sources*, **136**, 154 (2004).
60. F. F. Cao, Y. G. Guo, S. F. Zheng, X. L. Wu, L. Y. Jiang, and R. R. Bi et al., *Chemistry of Materials*, **22**, 1908 (2010).
61. G. Q. Liu, L. Wen, and Y. M. Liu, *Journal of Solid State Electrochemistry*, **14**, 2191 (2010).
62. Honda Motor Company. *Honda Motor Company*. www.honda.com, last accessed: May 2013.
63. Mitsubishi Motors Company. *Mitsubishi Motors Company*. http://www.mitsubishicars.com/MMNA/jsp/index.do, last accessed: May 2013.
64. Nissan Automotive Company. *Nissan USA*. http://www.nissanusa.com/, last accessed: May 2013.
65. Smart USA. *Smart USA*. http://www.smartusa.com/, last accessed: May 2013.
66. Tesla Motors. *Tesla Motors*. http://www.teslamotors.com/, last accessed: May 2013.
67. Toyota Motor Corporation. *Toyota Motor Corporation*. www.toyota.com, last accessed: May 2013.
68. Fiat USA. *Fiat*. www.fiatusa.com, last accessed: May 2013.
69. Ford Motor Company. *Ford Motor Company*. http://www.ford.com/, last accessed: May 2013.

Downloaded on 2014-11-13 to IP **128.95.145.3** address. Redistribution subject to ECS terms of use (see **ecsdl.org/site/terms_use**) unless CC License in place (see abstract).